

Fig. 8.

lengths for any scan direction  $\phi$  gives, of course, the area. First moments, combined with area, give the location of the centroid. Higher moments give shape parameters. If the moments (including area) are calculated at every scan angle, then the redundancy can be used to improve the accuracy.

A useful single parameter involving chord length is the maximum chord length which, as Fig. 8 shows, may be different from the maximum width. More detail is given by maximum chord length at each scan angle. Still more detail is given by all local maxima and minima.

### VIII. COMPLETE SHAPE INFORMATION

The various parameters and functions discussed in the previous sections all throw away some information about shape for the sake of simplicity. Complete information, i.e., information sufficient to reconstruct the image to within the quantization error, can be extracted in various ways. For example, if the sum of the lengths of the chords is kept separately for every scan line, then the image can be reconstructed by means of the Radon transform. For a time, it was conjectured that the distribution of chord lengths [5], [12], a location and orientation-independent data set easily obtained from the rotated scan, is also complete, but it has been shown that this is not the case [4]. The procedure outlined below provides a complete data set in a particularly convenient form.

First, find for each value of  $\phi$  the scan line that passes through the object's centroid. Second, locate on this scan line the endpoints of the object's chords relative to the centroid. This procedure provides a polar representation of the object with the origin at the centroid. It can be made scale independent by normalization with any scale-proportional parameter such as the perimeter, the maximum chord, or the square root of the area. It then requires only a one-parameter search (in  $\phi$ ) to match the normalized polar plot with a template. Even the one-parameter search can be eliminated if the polar plot and the templates can be oriented by means of an identifiable angle such as the angle of the maximum chord, the angle of the maximum width, or the angle of some other feature.

The two stages of the procedure can be carried out on two successive half rotations (in which case the locations of the scan lines through the centroid must be stored) or in a single half rotation (in which case the chord endpoint coordinates must be stored for the duration of each parallel scan).

This method is applicable, of course, primarily when it is known that the field of view contains only one object.

### REFERENCES

- [1] H. Freeman, "Shape characterization by the method of roving line segment scanning," summaries of presentations, IEEE Comput. Soc. Workshop on Pattern Recognition and Artificial Intell., Princeton, NJ, Apr. 1978.
- [2] A. Klinger, "Pattern width at a given angle," *Commun. ACM*, vol. 14, p. 21, 1971.
- [3] A. Klinger, A. Kochman, and N. Alexandridis, "Computer analysis of chromosome patterns, etc.," *IEEE Trans. Comput.*, vol. C-20, p. 1014, 1971.

- [4] C. L. Mallows and J. M. C. Clark, "Linear intercept distributions do not characterize plane sets," *J. Appl. Prob.*, vol. 7, p. 240, 1970.
- [5] D. J. H. Moore and D. J. Parker, "Analysis of global pattern features," *Pattern Recognition*, vol. 6, p. 149, 1974.
- [6] D. G. Nichol, "Hybrid optical digital computation of global chord functions," *Opt. Commun.*, vol. 43, no. 3, p. 168, 1982.
- [7] A. B. J. Novikoff, "Integral geometry as a tool in pattern perception," in *Principles of Self-Organization*, von Foerster and Zopf, Eds. New York: Pergamon, 1962, pp. 347-368.
- [8] T. Pavlidis, "Algorithms for shape analysis of contours and waveforms," *IEEE Trans. Pattern Anal. Machine Intell.*, vol. PAMI-2, p. 301, July 1980.
- [9] —, "A review of algorithms for shape analysis," *Comput. Graphics Image Processing*, vol. 7, p. 243, 1978.
- [10] A. Rosenfeld and A. C. Kak, *Digital Picture Processing*. New York: Academic, 1976.
- [11] G. Tenery, "A pattern recognition function of integral geometry," *IEEE Trans. Mil. Electron.*, vol. MIL-7, p. 196, 1963.
- [12] E. Wong and J. A. Steppe, "Invariant recognition of geometric shapes," in *Methodologies of Pattern Recognition*, S. Watanabe, Ed. New York: Academic, 1969, pp. 535-546.
- [13] C. T. Zahn and R. Z. Roskies, "Fourier descriptors for plane closed curves," *IEEE Trans. Comput.*, vol. C-21, p. 269, 1972.
- [14] M. G. Kendall and P. A. P. Moran, *Geometrical Probability*, Griffin's Statistical Monographs and Courses, no. 10. London, England: Griffin, 1963.
- [15] G. L. Miller and R. A. Boie, "A time-domain feature extraction method for machine vision using fixed fraction filters," presented at COMPCON '83, Crystal City, VA.

## Min-Max Operators in Texture Analysis

MICHAEL WERMAN AND SHMUEL PELEG

**Abstract**—A signature is generated for a given picture by operating on it with different masks. The operations are gray level generalizations of "shrink" and "expand" for binary pictures using Serra's morphological methods [10]. The signature is a set of numbers, each corresponding to an application of an operator at a certain scale and direction, and can be used to analyze the discriminate textures. It is shown that this family of signatures includes as special cases several currently used texture descriptors.

**Index Terms**—Min-max, morphological operators, texture analysis.

### I. INTRODUCTION

Serra defines dilation, erosion, opening, and closing of binary pictures, and uses these operators to measure morphological properties. These operations are generalized to gray level pictures and are used to analyze and classify textures.

#### A. Binary Definitions

Let  $P$  be a binary picture; the 1's represent the object, the 0's the background. If  $a = (a_x, a_y)$  are the coordinates of a pixel, then  $P_a$  is  $P$  translated by  $a$ , i.e.,  $P_a(x - a_x, y - a_y) = P(x, y)$ .

**Dilation:** Let  $A, B$  be binary pictures. The dilation of  $A$  by  $B$ ,  $D_{AB}$ , is defined as a binary picture, such that  $D_{AB}(a) = 1$  iff  $B_a$  and

Manuscript received July 10, 1984; revised May 23, 1985. Recommended for acceptance by S. W. Zucker. This work was supported in part by the National Science Foundation under Grant DCR-82-18408 and by a grant from the Israel National Council for Research and Development.

The authors are with the Center for Automated Research, University of Maryland, College Park, MD 20742, on leave from the Department of Computer Science, the Hebrew University of Jerusalem, 91904 Jerusalem, Israel.

$A$  have a nonempty intersection of their respective objects. Or, if  $f_p(a)$  is the characteristic predicate of  $P$ , being true iff the point  $a$  is in the object of  $P$ , then  $f_{D_{AB}}(a) = V_b\{f_A(b) \wedge f_B(b - a)\}$  (analogous to convolution). For example, if  $A = \begin{smallmatrix} 1 & 1 \\ 1 & 1 \end{smallmatrix}$  and  $B = \begin{smallmatrix} 1 & 1 \\ 1 & 1 \end{smallmatrix}$ , then

$$D_{AB} = \begin{smallmatrix} 1 & 1 \\ 1 & 1 \end{smallmatrix}.$$

*Erosion:* The erosion of  $A$  by  $B$ ,  $E_{AB}$ , is defined as the binary picture in which  $E_{AB}(a) = 1$  iff the object of  $B_a$  is totally included in the object of  $A$ . Using the characteristic predicate, we have  $f_{E_{AB}}(a) = \wedge_b\{f_A(b) \vee 1 \neg f_B(b - a)\}$ . Erosion is related to dilation through the following formulas.

$$\overline{E_{AB}} = D_{\overline{AB}}, \quad \overline{D_{AB}} = E_{\overline{AB}}.$$

For example, if  $A = 1111$  and  $B = 111$ , then  $E_{AB} = 11$ . Dilation results in enlarging the object in a pattern determined by the dilation matrix. Dilating an object with a matrix having only two 1's, for example, will result in duplicating the object at a distance equal to the distance between the 1's. Dilating with the matrix

$$\begin{smallmatrix} 1 & 1 \\ 1 & 1 \end{smallmatrix}$$

will add to the object all neighboring background elements. Erosion is the dilation of the background.

Opening and closing are two ways to compute "smooth" approximations of  $A$ . The closing of  $A$  by  $B$ ,  $C_{AB}$ , is defined as  $C_{AB} = E_{D_{AB}B}$ ;  $A$  is dilated by  $B$  and the result is eroded by  $B$ . The opening of  $A$  by  $B$  is defined by  $O_{AB} = D_{E_{AB}B}$ ;  $A$  is eroded by  $B$  and the result is dilated by  $B$ . Opening and closing are related through

$$\overline{O_{AB}} = C_{\overline{AB}}, \quad \overline{C_{AB}} = O_{\overline{AB}}.$$

In opening, the erosion causes partial reversal of the preceding dilation. In an object with holes, for example, after dilation the erosion can shrink the boundary back to its original shape, while holes that were completely filled by the dilation cannot be reclaimed.

## II. GRAY LEVEL GENERALIZATIONS

To generalize the operators from binary functions to gray level pictures, we give new meaning in dilation and erosion using fuzzy logic. In the binary case, dilation is defined by  $f_{D_{AB}}(a) = V_b\{f_A(b) \wedge f_B(b - a)\}$ ,  $f$  being the characteristic predicate. In fuzzy logic [14]  $V$  is replaced by maximum and  $\wedge$  is replaced by minimum. We will define  $D_{AB}$  where  $A$  and  $B$  are gray level pictures with values between 0 and 1, as

$$D_{AB}(a) = \sup_b \{\min(A(b), B(b - a))\}.$$

In the case that  $A$  and  $B$  are binary, this new definition is equivalent to the original binary definition. In the case that  $A$  is gray-level and  $B$  binary, then  $D_{AB}(a)$  is the maximum of all the values of  $A$  that coincide with the 1's of  $B_a$ .

Similarly, we define  $E_{AB}$  where  $A$  and  $B$  are gray level pictures as

$$E_{AB}(a) = \inf_b \{\max(A(b), 1 - B(b - a))\}.$$

If both  $A$  and  $B$  are binary, this definition is the same as the original binary definition. If  $A$  is a gray level function and  $B$  is binary,  $E_{AB}(a)$  is the minimum of all the values of the pixels of  $A$  that coincide with the 1's of  $B_a$ .

Using the new definitions for dilation and erosion, opening and closing are defined in the same way as the binary case:  $O_{AB} = D_{E_{AB}B}$  and  $C_{AB} = E_{D_{AB}B}$ .

Peleg and Rosenfeld [8] used these inf, sup (min, max) operators, with  $B$  being a digital ball with a radius of 1, to generalize shrink and expand from binary to gray level pictures. The gray level generalizations of the morphological operators described in this section are the same as Serra's [10] when  $A$  is a gray level picture

and  $B$  is binary. When  $A$  and  $B$  are both gray-level, Serra's definition is different: He defines erosion as  $\inf_b \{A(b) - B(a - b)\}$  and dilation as  $\sup_b \{A(b) + B(a - b)\}$ .

## III. GENERATION OF DESCRIPTORS

In this section, we develop families of operators on a picture (or part of a picture) that generate descriptor matrices.

Let  $P$  be a gray level picture. Define  $\sigma(P)$  as the sum of the gray level values of the pixels in  $P$ . Let  $\{M_{r,\omega}\}$  be a set of masks with parameters  $r \in R$ ,  $\omega \in \Omega$ . One possible choice for  $M_{r,\omega}$  is to be a straight line segment of length  $r$  and angle  $\omega$  ( $r \geq 0$ ,  $0 \leq \omega < \pi$ ). For example,

$$M_{3,\pi/4} = \begin{smallmatrix} & & 1 \\ & 1 & \\ 1 & & \end{smallmatrix} \quad \text{and} \quad M_{2,0} = \begin{smallmatrix} 1 & 1 \\ 1 & 1 \end{smallmatrix}.$$

Using the set of masks  $\{M_{r,\omega}\}$ , we define four feature matrices for a picture  $P$ .

- 1) The dilation matrix  $D = (\sigma(D_{PM_{r,\omega}}))$ .  $D(r, \omega)$  is the sum of the pixels in the picture generated by the dilation of  $P$  by  $M_{r,\omega}$ .
- 2) The erosion matrix  $E = (\sigma(E_{PM_{r,\omega}}))$ .  $E(r, \omega)$  is the sum of the pixels in the picture generated by the erosion of  $P$  by  $M_{r,\omega}$ .
- 3) The closing matrix  $K = (\sigma(C_{PM_{r,\omega}}))$ .  $K(r, \omega)$  is the sum of the pixels in the picture generated by the closing of  $P$  by  $M_{r,\omega}$ .
- 4) The opening matrix  $O = (\sigma(O_{PM_{r,\omega}}))$ .  $O(r, \omega)$  is the sum of the pixels in the picture generated by the opening of  $P$  by  $M_{r,\omega}$ .

Other choices for  $M_{r,\omega}$  are possible. An example is a binary mask of a rectangle (including its interior) whose sides are parallel to the axis and whose diagonal is of length  $r$  and angle  $\omega$ . For example,

$$M_{3,\pi/4} = \begin{smallmatrix} 1 & 1 & 1 \\ 1 & 1 & 1 \\ 1 & 1 & 1 \end{smallmatrix} \quad \text{and} \quad M_{4,\arctg 1/3} = \begin{smallmatrix} & & 1 & 1 & 1 & 1 \\ & & & 1 & 1 & 1 \\ & & & & 1 & 1 \\ & & & & & 1 \\ 1 & 1 & 1 & & & \end{smallmatrix}.$$

Given a picture  $P$  for any type of mask  $M_{r,\omega}$  and sets  $R$  and  $\Omega$  of lengths and angles, the four feature matrices can be generated. Every matrix measures some property of  $P$ . The use of these matrices will be described in Section IV. For simplicity, in the rest of this correspondence, only straight line segments will be used for masks.

## IV. SIGNATURES

We can use one or more of the erosion, dilation, opening, and closing matrices in order to define a signature for a picture. These features for masks of line segments can be as follows.

- 1) The entire matrix. These matrices measure the effect of an operation (erosion, dilation, opening, or closing) with different masks. When features of size  $l$  occur at angle  $\omega$ , operations with line segments of length  $l$  and angle  $\omega$  will reveal strong effects. In a texture of vertical black lines distance  $d$  apart, for example, opening with horizontal line masks will do nothing when the line segments are shorter than  $d$ , but the entire picture will become black when the line segments are longer than  $d$ .

- 2) Sums of rows over all angles. This corresponds to the overall effect of all line segments of equal length, and measures features regardless of their orientation. The row sum for length  $l$  in  $O$  indicates the existence of objects of size  $l$ , while the row sum for length  $l$  in  $K$  indicates the existence of "holes" of size  $l$ .

- 3) Sums of columns over all lengths. This corresponds to the overall effect of all line segments of the same orientation, and measures orientation features of all spatial sizes.

Measuring the different responses to different masks demonstrates the effect of small changes in mask size. Derivatives are helpful in finding critical size masks. For example, for the opening matrix  $O$  as follows.

- 4) The derivative by row  $O(r, \omega) - O(r, \omega - 1)$  measures the change caused by changing the angle of the line segment.

5) The derivative by column  $\mathbf{O}(r, \omega) - \mathbf{O}(r - 1, \omega)$  measures the change caused by changing the length of the line segment.

6) The gradient  $|\mathbf{O}(r, \omega) - \mathbf{O}(r - 1, \omega - 1)| + |\mathbf{O}(r - 1, \omega) - \mathbf{O}(r, \omega - 1)|$  measures the change caused by changing the angle and the length of the line segment. An example of the use of these derivatives will be given in Section V-A.

In order to compare two pictures, we compare some of their respective signatures. This can be done, for example, by summing up all the absolute differences of their corresponding feature matrices. More meaningful comparisons (but using more computation) can be obtained with generalizations of the distance measures suggested in [3] and [15]. This metric is a generalization of the metric suggested in [12], and involves computing a minimal matching between the features. Further details, as well as proofs, can be found in [15] and [3].

V. RELATION TO OTHER METHODS

Several known operators are instances of the erosion and dilation described in this correspondence, especially in the binary case.

A. Binary Run Lengths

A run length primitive is a maximal collinear connected set of pixels in the object. A run length primitive can be characterized by its length and its angle. Galloway [4], [5] used these primitives to categorize textures.

Let  $M_{r,\omega}$  be a line segment of length  $r$  and angle  $\omega$ , and let  $P$  be a binary picture. The  $(r, \omega)$  entry in the second derivative by column of the erosion matrix  $E$  is exactly the number of run length primitives of length  $r$  and angle  $\omega$  in  $P$ . Each run length primitive of length  $r$  and angle  $\omega$  adds 1 to  $E(r, \omega)$ , 2 to  $E(r - 1, \omega)$ , 3 to  $E(r - 2, \omega)$ , and so on. For example, let

$$\begin{array}{l}
 P = 0 \ 1 \ 1 \ 1 \ 1 \ 0 \ 1 \ 1 \ 0 \\
 E_{P,M_{1,0}} = 0 \ 1 \ 1 \ 1 \ 1 \ 0 \ 1 \ 1 \ 0, \quad E(1, 0) = \sigma(E_{P,M_{1,0}}) = 6 \\
 E_{P,M_{2,0}} = 0 \ 1 \ 1 \ 1 \ 0 \ 0 \ 1 \ 0 \ 0, \quad E(2, 0) = \sigma(E_{P,M_{2,0}}) = 4 \\
 E_{P,M_{3,0}} = 0 \ 1 \ 1 \ 0 \ 0 \ 0 \ 0 \ 0 \ 0, \quad E(3, 0) = \sigma(E_{P,M_{3,0}}) = 2 \\
 E_{P,M_{4,0}} = 0 \ 1 \ 0 \ 0 \ 0 \ 0 \ 0 \ 0 \ 0, \quad E(4, 0) = \sigma(E_{P,M_{4,0}}) = 1 \\
 E_{P,M_{5,0}} = 0 \ 0 \ 0 \ 0 \ 0 \ 0 \ 0 \ 0 \ 0, \quad E(5, 0) = \sigma(E_{P,M_{5,0}}) = 0.
 \end{array}$$

Therefore,  $E = (6, 4, 2, 1, 0, 0, \dots)$ , and the derivative of  $E$  by row is

$$E' = (2, 2, 1, 1, 0, 0, \dots)$$

while the second derivative is

$$E'' = (0, 1, 0, 1, 0, 0, \dots)$$

The 1's at locations 2 and 4 stand for one run length primitive of length 2 and one of length 4 in  $P$ .

B. Binary Autocorrelation

The autocorrelation function is commonly used in texture utilizing the linear dependence of the pixels [5], [11]. The autocorrelation of  $P$  is  $A(r, \omega) = \sum_a P(a) P_{r,\omega}(a)$  where  $P_{r,\omega}$  is  $P$  translated by  $(r \cos(\omega), r \sin(\omega))$ .

The autocorrelation  $A(r, \omega)$  of a binary picture  $P$  is the erosion matrix  $E$  of  $P$  by matrices  $M_{r,\omega}$  where  $M_{r,\omega}$  are the two endpoints of line segments of length  $r$  and angle  $\omega$ . This follows from the fact that the product of two binary digits is the same as their minimum.

C. Multiple Resolution Texture Analysis

In order to classify textures, Peleg *et al.* [7] measured changes in their properties with changing resolution. Treating gray levels as elevations, the surface area of the gray level surface was measured at several resolutions. This area decreases at coarser resolutions, since the fine details that contribute to the area disappear. The rate of this decrease in area was used for texture comparison and classification. The surface area at different resolutions was computed

in [7] by dilating the gray level surface with three-dimensional (3-D) digital balls of different sizes, and dividing the resulting volume by the radius of the ball. The derivative of the dilation matrix  $D$  (and the erosion matrix  $E$ ) by squares of different sizes is very similar to the rate of decrease of surface area, and has the same experimental classification power as the methods in [7].

VI. COMPUTATIONAL COMPLEXITY

In order to compute the dilation matrix  $D(r, \omega) = (\sigma(D_{M_{r,\omega}}))$ ,  $r \in R, \omega \in \Omega$ , we do not always have to dilate the picture separately for each mask. We describe several computation methods for the dilation matrix which are also applicable for erosion. Unfortunately, most methods will not help speed up the computation of opening or closing. Special architecture, however, is available to speed up this computation [8].

Often, dilation by large elements can be achieved by iterative application of smaller elements. Dilation by straight lines, for example, can be reached by iterative dilation with line segments of length 2. When dilations by all intermediate lengths are needed, this method is more efficient than direct dilation by all lengths. Similar speed improvements are possible for dilation by rectangles.

When dilation by a large element is needed, a different method is to precompute for each pixel the closest pixels on the same line that are bigger or equal to it in value. Having this information, we can compute for how many different length line segments this pixel is the maximum. The precomputation step takes  $O(|P| \log |P|)$ , using the range finding methods of Bentley [1]. A similar approach is applicable to rectangles where the use of quad trees and oct trees [9], [6] is efficient for the precomputation.

A fast algorithm for computing the dilation of a picture  $P$  by any binary mask exists. It is sketched here for the case where the binary

mask is a line segment of length  $k$  and angle  $O$ , and  $P$  is a one-dimensional picture.

Let  $H$  be a heap with an auxiliary queue  $Q$  with pointers to  $H$ .

1) *Initialization*: Build the heap  $H$  and the queue  $Q$  so that  $H$  has the first  $k$  elements of  $P$ , its apex is its maximum, and  $Q$  has  $k$  elements where the  $i$ th element is a pointer to the location of the  $i$ th element of  $P$  on the heap.

2) *Output*: Output the apex of the heap.

3) *Output*: Remove the end of  $Q$  and the entry on the heap it points to. Insert the next element of  $P$  into  $H$  and put its address at the beginning of  $Q$ .

4) Go to 2 until  $P$  is finished.

The computation is correct because the heap will always have at its apex the maximum of the last  $k$  elements.

The complexity is  $O(k)$  for the first step,  $O(1)$  for the second and  $O(\log(k))$  for the third, or altogether  $O(|P| \log(k))$  for the entire computation.

The same can be done for erosion. Similar algorithms using two heaps can be used to compute an opening or a closing.

VII. APPLICATIONS TO TEXTURE CLASSIFICATION

This section will describe some experiments in the application of the proposed measures to texture analysis. Fourteen different texture pictures from Brodatz [17] were used: beans, burlap, cork, grass, marble, mica, paper, pellets, pigskin, raffia, rice paper, seafan, straw, and bark. Two different  $64 \times 64$  windows were taken from each texture.

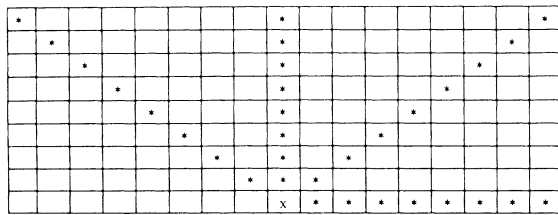


Fig. 1. The line segments used in the experiments. Four directions were used, and in each direction eight different lengths were tested. There is no need to use the directions in the other half of the circle, as their effect is obtained by using these four directions.

TABLE I

THE EROSION MATRICES OF BEANS, BURLAP, AND CORK. THE COLUMNS REPRESENT DIFFERENT ANGLES, WHILE THE ROWS REPRESENT DIFFERENT SEGMENT LENGTHS. ALL RESULTS WERE NORMALIZED TO THE GRAY LEVEL OF THE ORIGINAL IMAGE TO GIVE 100 IN THE FIRST ROW

Erosion of beans					Erosion of burlap					Erosion of cork				
	0	$\frac{\pi}{4}$	$\frac{\pi}{2}$	$\frac{3\pi}{4}$		0	$\frac{\pi}{4}$	$\frac{\pi}{2}$	$\frac{3\pi}{4}$		0	$\frac{\pi}{4}$	$\frac{\pi}{2}$	$\frac{3\pi}{4}$
0	100	100	100	100	0	100	100	100	100	0	100	100	100	100
1	89	86	90	87	1	86	79	86	82	1	93	92	95	93
2	79	75	81	75	2	75	64	75	67	2	88	86	91	88
3	70	65	73	64	3	66	51	69	56	3	83	81	88	85
4	62	58	66	55	4	60	43	66	48	4	79	77	86	82
5	54	52	59	47	5	55	37	63	43	5	75	73	83	80
6	48	47	54	40	6	51	33	61	40	6	71	69	81	78
7	42	43	49	35	7	48	30	59	38	7	68	66	80	77
8	37	39	45	31	8	45	27	57	36	8	65	63	78	75

The erosion matrix  $E$  was generated by eroding the images with straight line segments. The line segments was of 4 directions and 8 lengths, totaling 32 different segments. The structure of the segments is displayed in Fig. 1, and erosion matrices of three different textures are displayed in Table I.

Examination of the erosion matrices reveals that after erosion with yardsticks of length eight (last row), the cork matrix preserves the highest values among the three matrices. Since the dilation is a local minimum operator, this phenomenon could be caused by the low contrast of the cork, compared to the higher contrast of the beans and burlap.

More useful information can be obtained from the erosion matrices by using their derivatives relative to the yardstick. Such descriptors are displayed in Table II, and are the columnwise derivatives of the matrices in Table I. Examination of the burlap matrix reveals strong directional effects with yardsticks of length 1-5 where the derivative for the 0 and  $\pi/2$  directions is much lower than that for directions  $\pi/4$  and  $3\pi/4$ . For larger yardsticks, the directionality disappears. This exhibits the usefulness of similar matrices in revealing the interdependency between directionality and scale.

For discrimination purposes, the erosion matrices were compared to each other. All 28 matrices (two for each texture) were compared, and the distance computed between each pair. Partial results of this comparison are displayed in Table III. Of the 28 matrices, all but one were closest to the second matrix of the same texture. The same matrix comparison has been performed for the derivatives of the erosion matrices, giving perfect results. Using the dilation matrices gave again one misclassification, different from the one of the erosion matrices.

These descriptors are thus shown to be powerful for texture discrimination. For a given application, one has a choice of using any of the many descriptors available, each descriptor exhibiting a different aspect of the texture.

VIII. CONCLUDING REMARKS

A new set of morphological image features is proposed, and is shown experimentally to be of value in texture analysis. These features measure combined effects of directionality and scale. It has been shown that some previously used descriptors are special cases of the general descriptors suggested here.

TABLE II

DERIVATIVE BY COLUMNS OF THE EROSION MATRICES. THE ELEMENTS IN THE  $i$ TH ROW ARE THE EROSION MATRICES OF THE VALUES IN THE  $i$ -ST AND  $i$ TH ROWS

Erosion derivatives of beans					Erosion derivatives of burlap					Erosion derivatives of cork				
	0	$\frac{\pi}{4}$	$\frac{\pi}{2}$	$\frac{3\pi}{4}$		0	$\frac{\pi}{4}$	$\frac{\pi}{2}$	$\frac{3\pi}{4}$		0	$\frac{\pi}{4}$	$\frac{\pi}{2}$	$\frac{3\pi}{4}$
1	11	14	10	13	1	14	21	14	18	1	7	8	5	7
2	10	11	9	12	2	11	15	11	15	2	5	6	4	5
3	9	10	8	11	3	9	13	6	11	3	5	5	3	3
4	8	7	7	9	4	6	8	3	8	4	4	4	2	3
5	8	6	7	8	5	5	6	3	5	5	4	4	3	2
6	6	5	5	7	6	4	4	2	3	6	4	4	2	2
7	6	4	5	5	7	3	3	2	2	7	3	3	1	1
8	5	4	4	4	8	3	3	2	2	8	3	3	2	2

TABLE III

TEXTURE CLASSIFICATION. PARTIAL RESULTS OF COMPARING ALL 28 TEXTURE WINDOWS. ELEMENTS IN THE MATRIX ARE THE DIFFERENCES BETWEEN THE RESPECTIVE EROSION MATRICES. IN THIS SUBSAMPLE, EVERY TEXTURE HAS AN EROSION MATRIX MOST SIMILAR TO THE OTHER SAMPLE OF THE SAME TEXTURE. IN THE FULL COMPARISON, ONE TEXTURE SAMPLE WAS MISCLASSIFIED. THE MINIMUM IN EACH COLUMN AND EACH ROW IS BARRED

	beans2	burlap1	cork1	mica1	paper1	pellets1	pig1	raffia1
beans2	5	13	21	12	14	8	18	15
burlap2	9	<u>5</u>	21	16	16	10	19	18
cork2	25	26	<u>1</u>	11	8	28	3	7
mica2	14	17	11	<u>1</u>	6	17	8	6
paper2	17	21	7	6	<u>1</u>	20	4	5
pellets2	6	13	25	15	17	<u>3</u>	22	19
pig2	22	24	2	8	6	25	<u>1</u>	5
raffia2	17	19	7	5	5	20	6	<u>1</u>

REFERENCES

- [1] J. I. Bentley and H. A. Maurer, "Efficient worst case data structures for range searching," *Acta Informatica*, vol. 13, pp. 155-168, 1980.
- [2] P. Brodatz, *Textures*. New York: Dover, 1966.
- [3] M. Werman, S. Peleg, and A. Rosenfeld, "A distance metric for multidimensional histograms," Center Automat. Res., Univ. Maryland, College Park, MD, Tech. Rep. TR-90, Aug. 1984.
- [4] M. Galloway, "Texture analysis using gray level run lengths," *Comput. Graph. Image Processing*, vol. 4, pp. 172-199, 1974.
- [5] R. M. Haralick, "Statistical and structural approaches to textures," *Proc. IEEE*, vol. 67, pp. 786-804, 1979.
- [6] C. L. Jackins and S. L. Tanamoto, "Octrees and their use in representing three-dimensional objects," *Comput. Graph. Image Processing*, vol. 14, pp. 249-270, 1980.
- [7] S. Peleg, J. Naor, R. Hartley, and D. Avnir, "Multiple resolution texture analysis and classification," *IEEE Trans. Pattern Anal. Machine Intell.*, vol. PAMI-6, pp. 518-523, 1984.
- [8] S. Peleg and A. Rosenfeld, "A min-max medial axis transformation," *IEEE Trans. Pattern Anal. Machine Intell.*, vol. PAMI-3, no. 2, pp. 206-210, 1981.
- [9] H. Samet, "Connected component labelling using quadtrees," *J. ASS. Comput. Mach.*, vol. 28, pp. 487-501, 1981.
- [10] J. Serra, *Image Analysis and Mathematical Morphology*. London, England: Academic, 1982.
- [11] J. Weszka, C. Dyer, and A. Rosenfeld, "A comparative study of texture measures for terrain classification," *IEEE Trans. Syst., Man, Cybern.*, vol. SMC-6, pp. 269-285, 1976.
- [12] A. K. C. Wong and H. C. Shen, "Search-effective multiclass texture classification," in *Proc. IEEE Conf. Pattern Recognition Image Processing*, 1982, pp. 208-213.
- [13] K. J. Supowit and E. M. Reingold, "Divide and conquer heuristics for minimum weighted Euclidean matching," *SIAM J. Comput.*, vol. 12, pp. 118-143, 1983.
- [14] L. A. Zadeh, *Fuzzy Sets and their Applications to Cognitive Processes*. New York: Academic, 1975.
- [15] M. Werman, S. Peleg, R. Melter, and T. Y. Kong, "Bipartite graph matching for points on a line or a circle," *J. Algorithms*, in press.
- [16] S. R. Sternberg, "Biomedical image processing," *IEEE Trans. Comput.*, vol. C-16, pp. 22-34, Jan. 1983.